NANO LETTERS

Letter

pubs.acs.org/NanoLett

Scalable Quantum Photonics with Single Color Centers in Silicon Carbide

Marina Radulaski,[*,†] Matthias Widmann,[*,‡] Matthias Niethammer,[‡] Jingyuan Linda Zhang,[†] Sang-Yun Lee,[‡,§] Torsten Rendler,[‡] Konstantinos G. Lagoudakis,[†] Nguyen Tien Son,[∥] Erik Janzén,[∥] Takeshi Ohshima,[⊥r] Jörg Wrachtrup,[‡] and Jelena Vučković[†]

[†]E. L. Ginzton Laboratory, Stanford University, Stanford, California 94305, United States

[‡]3rd Institute of Physics, IQST, and Research Center SCOPE, University of Stuttgart, 70569 Stuttgart, Germany

[§]Center for Quantum Information, Korea Institute of Science and Technology (KIST), Seoul, 02792, Republic of Korea

[∥]Department of Physics, Chemistry, and Biology, Linköping University, SE-58183 Linköping, Sweden

[⊥r]National Institutes for Quantum and Radiological Science and Technology (QST), Takasaki, Gunma 370-1292, Japan

Supporting Information

ABSTRACT: Silicon carbide is a promising platform for single photon sources, quantum bits (qubits), and nanoscale sensors based on individual color centers. Toward this goal, we develop a scalable array of nanopillars incorporating single silicon vacancy centers in 4H-SiC, readily available for efficient interfacing with free-space objective and lensed-fibers. A commercially obtained substrate is irradiated with 2 MeV electron beams to create vacancies. Subsequent lithographic process forms 800 nm tall nanopillars with 400−1400 nm diameters. We obtain high collection efficiency of up to 22 kcounts/s optical saturation rates from a single silicon vacancy center while preserving the single photon emission and the optically induced electron-spin polarization properties. Our study demonstrates silicon carbide as a readily available platform for scalable quantum photonics architecture relying on single photon sources and qubits.

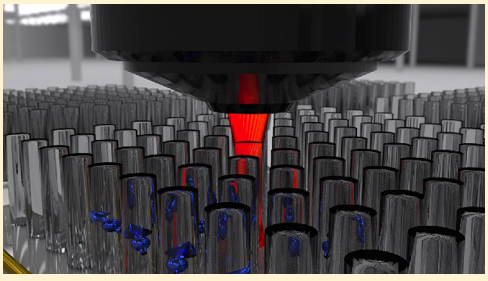

KEYWORDS: *Color centers, silicon carbide, photonics, spintronics, nanopillars, spin-qubits*

Silicon carbide (SiC) has recently emerged as a host of color centers with exceptional brightness[1] and long spin coherence times,[2−5] much needed for the implementations of solid-state quantum bits and nanoscale magnetic sensors.[6] In addition to a favorable set of physical properties, such as the wide band gap and high index of refraction, this material also benefits from the decades of utilization in power electronics;[7] wafer scale substrates available for purchase, doping, and various etching processes[8−11] are at an engineer's disposal. This makes SiC advantageous over diamond and rare-earth doped crystals for industrial applications in quantum computing and sensing, as well as for integration of point defects with electronics and CMOS devices. Electron spins of various SiC color center ensembles have been coherently controlled to date.[3,12,13] We focus our attention on individual silicon vacancy (V_{Si}) centers in 4H-SiC, whose electron spin was recently employed as room temperature qubit;[2] the first one is at the single defect level in SiC. This system features spin coherence times of at least 160 μs and with a potential for improvement through isotopic purification. To bring this system closer to the applications, we address V_{Si}/4H-SiC platform from the points of scalability, device footprint, optical interface, and collection efficiency, while preserving optically induced electron-spin polarization properties.

Our platform consists of a 2D array of simultaneously fabricated nanopillars in electron beam irradiated 4H-SiC. The nanopillars feature 0.16−2 μm^2 footprint and efficient signal collection from single color centers into a free space objective of NA = 0.65. Such numerical aperture is also available among lensed fibers,[14] as a potential alternative interface. In comparison, a previous approach has relied on the nonscalable fabrication of solid immersion lens (SIL) interface.[2] Here, focused ion-beam milling with heavy ions is used, and an intense combination of wet and reactive ion etching needs to be performed to remove radiation damage in the SiC lattice. A footprint of an individual SIL is ∼1000 μm^2. In another approach, a bulk wafer was irradiated to generate a 2D array of color center sites.[15] Both of these approaches relied on collection into high numerical aperture (NA = 1.3) oil immersion lens in direct contact with the substrate. Vertically directed waveguiding in nanopillars allowed us to observe up to 22 kcounts/s (kcps) collection from single color centers with half the NA value. This is comparable to the best previous result of 40 kcps achieved in a nonscalable system[2] and a 3-fold

Received: December 8, 2016
Revised: February 21, 2017
Published: February 22, 2017

DOI: 10.1021/acs.nanolett.6b05102
Nano Lett. XXXX, XXX, XXX−XXX

increase over 7 kcps result in a scalable array in bulk.[15] The use of NA = 0.95 air objective lens would result in a few-fold increase in collection efficiency, as discussed in Supporting Information. We also observe 2−4% relative intensity in optically detected magnetic resonance (ODMR), comparable to the previous result.[2] Finally, the preservation of optical and spin properties of V_{Si} centers makes this platform applicable for wafer-scale arrays of single photon sources and spin-qubits.

Fabrication. We develop a scalable nanofabrication process, based on electron irradiation and electron beam lithography, which produces tens of thousands of nanopillars per squared millimeter in 4H-SiC substrate that incorporates V_{Si} color centers. Figure 1a illustrates the process flow. The initial sample

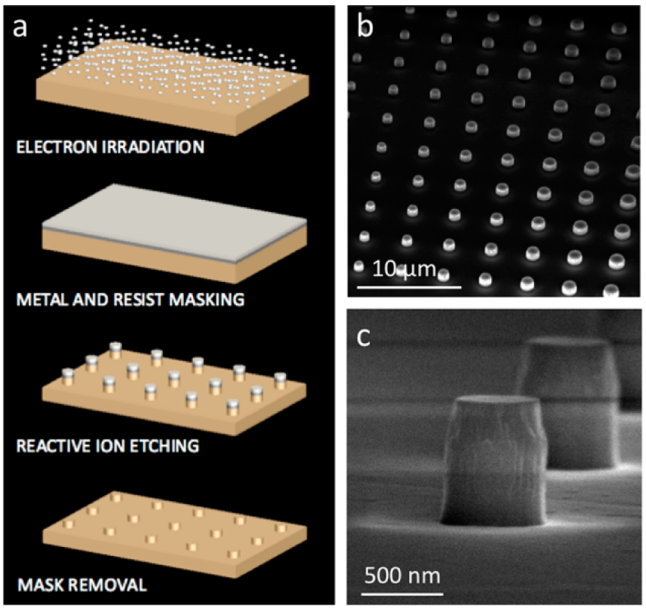

Figure 1. (a) Lithographic process for fabrication of nanopillars in 4H-SiC. (b) SEM images of fabricated array of nanopillars with variable diameters. (c) SEM image of a 600 nm wide and 800 nm tall nanopillar.

is a commercially available high purity semi-insulating 4H-SiC crystal, irradiated with 2 MeV electrons at a fluence of 10^{14} cm^{-2} at room temperature. For the purposes of hard etch mask, 300 nm of aluminum was evaporatively deposited onto the sample. Microposit ma-N negative tone resist was spun over it for patterning of nanopillars in 100 keV JEOL (JBX-6300-FS) electron beam lithographic system. Aluminum hard mask was etched in Cl_2 and BCl_3 plasma, and the pattern was transferred to silicon carbide in an SF_6 plasma process, both performed in the Versaline LL-ICP Metal Etcher. The mask was stripped in KMG Aluminum Etch 80:3:15 NP.

The pattern consists of 10 × 10 arrays of nanopillars with 5 μm pitch and diameters varied between 400 nm and 1.4 μm. The profile features 800 nm tall cylinder whose upper third has a shape of a cone frustum, reducing the top diameter by 120 nm. Figure 1b,c shows the SEM images of the fabricated structures.

Collection Efficiency. We model emission of color centers placed in pillars using finite-difference time-domain method. Index of refraction distribution is made according to the profile of fabricated pillars (n_{SiC} = 2.6, n_{air} = 1) and continuous wave dipole excitation at 918 nm is positioned within. We consider nanopillars of 400−1400 nm diameter with excitation at the central axis of the pillar (r = 0, z = 400 nm) with in-plane (E_r) and vertically oriented (E_z) dipole components. The orientation of V_{Si} dipole in our samples is along main crystal axis which forms $\theta = 4°$ angle with z-axis, and therefore we add the components to obtain total collected field $E = E_z \cos\theta + E_r \sin\theta$ (Figure 2a). We evaluate the fraction of collected emission by a two-step analysis. First, we monitor the power that penetrates the walls of the simulation space and evaluate the fraction of light that is emitted vertically upward (Figure 2b). Next, we analyze the far-field image (Figure 2c) and obtain the power fraction of vertically emitted light that is collected within a given numerical aperture (NA). Because of the dominant contribution of the dipole-component along the z-axis, which is also noticeable in Figure 2a, we consider only vertical excitation E_z for additional analyses (details in Supporting Information). In an extensive search for the optimal dipole-emitter position for each pillar diameter, we learn that color center positioning closer to the bottom of the pillar is advantageous for collection efficiency. We also run this analysis for unpatterned silicon carbide in order to estimate the expected collection efficiency increase achieved through nanopillar waveguiding, which yields 1−2 orders of magnitude improvement. The results are presented in Figure 2d,e showing favorable collection efficiency of 600 nm and 1000 nm diameter nanopillars.

Single Photon Emission. Photoluminescence (PL) measurements obtained in a home-built confocal microscope at room temperature are shown in Figure 3. Light from a single-mode laser diode operating at 730 nm was sent to an air objective (Zeiss Plan-Achromat, 40×/0.65 NA) in order to excite the defects. The PL signal was collected with the same objective and sent through a dichroic mirror and subsequently spatially filtered by a 50 μm diameter pinhole. The photons emitted by the defects were spectrally filtered by a 905 nm long pass filter and finally collected with two single photon counting modules in a Hanburry−Brown−Twiss configuration or, alternatively, with a spectrometer (details presented in Supporting Information). The density of color centers is too high to resolve single defects in the bulk crystals with no fabricated structures, however, combined with the nanopillars, a spatial separation of single defects is possible, simultaneously providing a moderate yield of defects placed in the pillars, as shown in Figure 3a. Approximately 4 out of 100 pillars host single V_{Si} defects which have desirable lateral and vertical placement and show an enhanced photon count-rate compared to defects without photonic structure.[15] For each investigated V_{Si} defect, a laser power-dependent saturation curve of the PL was collected as shown in Figure 3b. The background was obtained by collecting the light from an empty pillar nearby and subtracted from the defects emission. The influence of the diameter was experimentally examined by a statistical analysis of the maximum PL intensity as a function of the diameter. The maximum PL was obtained by fitting the background-corrected saturation curve with a power law: $I(P) = \frac{I_s}{1 + \alpha / P}$, where I is the PL intensity as a function of the excitation power P, α is excitation power when saturated and I_s denotes the saturation photon count-rate. The result of the fit parameter I_s is plotted as a function of the diameter in Figure 3c and shows a qualitative match to the modeled collection efficiency trend. The error bars were obtained by the error from the least-squares fits. The maximum PL from a single defect was found in the pillars with 600 nm diameter, showing I_{max} = 22 kcps, which is an increase of factor of 2−3 compared to 5−10 kcps

DOI: 10.1021/acs.nanolett.6b05102
Nano Lett. XXXX, XXX, XXX−XXX

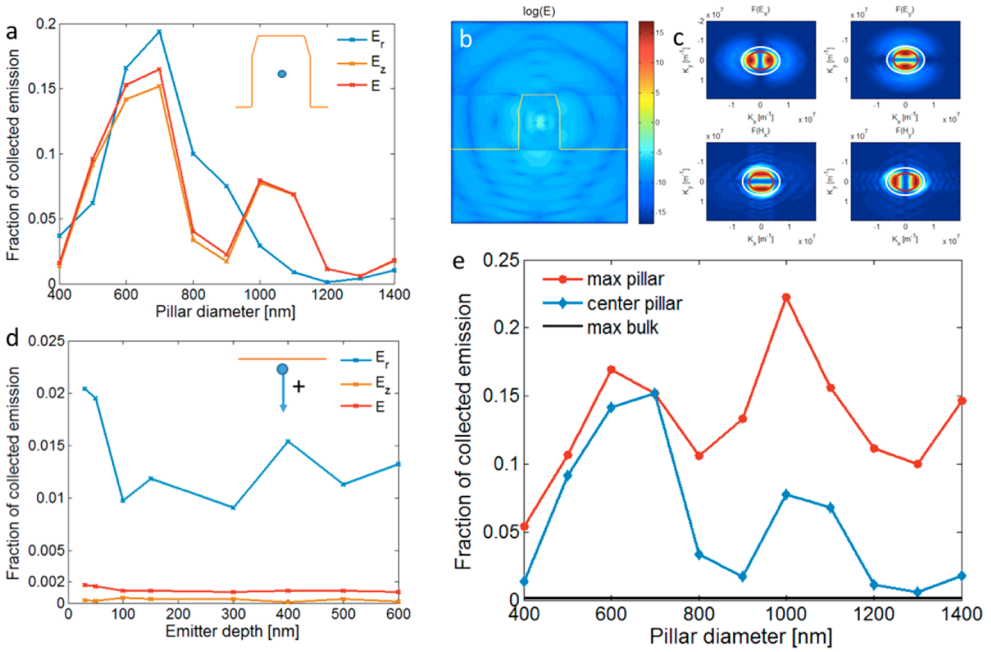

Figure 2. (a) Collection efficiency from a dipole emitter positioned at the center of 800 nm tall SiC nanopillar (indicated by inset drawing) with 4° offset from *z*-axis (red), plotted with its vertical (yellow) and radial (blue) components. (b) Finite difference time domain model of electric field propagation from a dipole emitter placed in the center of a 600 nm wide nanopillar. (c) Far-field emission profile of (b) with light line (white) and NA line (red). (d) Color center depth dependence of collection efficiency from a dipole emitter in bulk SiC with components marked as in (a); inset drawing illustrates the direction of increasing depth. (e) Diameter dependence of optimal (red) and centrally (blue) positioned color center in nanopillar, showing up to 2 orders of magnitude higher collection efficiency compared to bulk value of 0.0017.

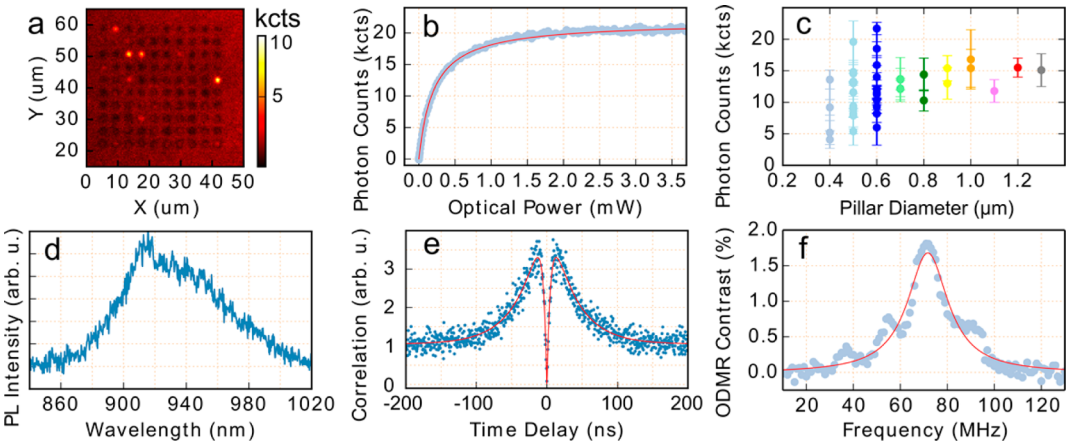

Figure 3. (a) Photoluminescence intensity map of a block of pillars. (b) PL intensity of a single V_{Si} as a function of the optical power, saturating at 22 kcps. The red line shows a fit to the data. (c) Diameter-dependent collected count rate. (d) Typical room-temperature PL spectrum of a single V_{Si} emitter in a nanopillar. (e) Typical second order correlation function showing antibunching at zero time delay, a clear evidence for single photon emission. The red line shows a double exponential fit to the data (details in Supporting Information). (f) ODMR signal from a single V_{Si} in a nanopillar. The red line shows a Lorentzian fit to the data.

for a single V_{Si} defect without photonic structures reported in literature.[2,15,16] This increase is smaller than expected from the model, which is attributed to the imperfect fabrication profile. A typical room-temperature PL spectrum is shown in Figure 3d, whereas Figure 3e shows a typical second order autocorrelation measurement with a clear single photon emission characteristic.

Single Spin Optically Detected Magnetic Resonance at Room Temperature. In order to address the single spins, a radio frequency (RF) signal was generated by a Rohde and Schwarz vector signal generator, subsequently amplified and applied to the V_{Si} in pillars through a 25 μm copper wire, which was spanned over the sample. Detailed information about the experimental methods for ODMR are described in a previous publication.[2] Continuous wave (cw) ODMR is observable under cw laser excitation where spin-dependent transitions over a metastable state lead to a spin polarization into the magnetic sublevels. At the same time, RF is swept over the spin resonance. When the RF signal is resonant to the Larmor-frequency, the spin state is changed and the transition rates over the metastable state is altered, hence a change in PL intensity can be detected. About 10% of the single V_{Si} defects that show enhanced emission also showed clear spin imprints, as illustrated in a typical ODMR measurement at a zero magnetic field plotted in Figure 3f, which is in agreement with

DOI: 10.1021/acs.nanolett.6b05102
Nano Lett. XXXX, XXX, XXX−XXX

previous studies.[2,15] V_{Si} defects in 4H-SiC can originate from two inequivalent lattice sites.[17] Among them, the so-called V2 center can be identified by their 70 MHz zero-field splitting[18] of the ground state spin of S = 3/2. The center position at 70 MHz of a broadened ODMR spectrum as shown in Figure 3f confirms that the found V_{Si} defects showing ODMR signals are V2 centers. The side-peaks surrounding the center-frequency originate from a nonzero parasitic magnetic field oriented in an arbitrary direction in the experimental environment, which is typically about 0.2−0.6 G.[19,20] The peak at 40 MHz can often be observed, also in other samples,[17] but further investigation of the origin is not in the scope of this work. The relative intensity of ODMR was calculated as $(PL_{on} - PL_{off})/PL_{off}$ and it varies between 2%−4%, which is in good agreement with previous single spin studies.[2,15]

In conclusion, we have developed a scalable and efficient platform for collecting single silicon vacancy color center emission in silicon carbide through a free space objective or a lensed fiber interface, applicable for single photon generation and coherent control of spin-qubits. This platform presents an improvement in terms of scalability, device footprint, and optical interface while providing competitive collection efficiency. The approach can be extended to incorporate other color centers in bulk 3C-, 4H-, and 6H-SiC samples.[1,3,13,21,22] In addition, silicon carbide is a biocompatible substrate[23] and can be directly interfaced with cells for potential magnetic[16,19,24] and temperature sensing applications,[4] whose proof-of-principle have recently been reported. Ideas for future development include increasing collection efficiency by fabricating taller nanopillars, isotopic purification of the sample for accessing qubits with longer spin coherence times, and integration with microwave control on chip. Another exciting direction is the investigation of recently suggested spin−photon interface protocols based on the V_{Si} in SiC[25] that requires the enhanced photon collection efficiency and the drastically improved ODMR signal of the V_{Si} defects, which can be accessed at cryogenic temperatures.[26] There are several ways the irradiation could be modified to achieve a higher yield of pillars with preferentially positioned single emitters. Control over the depth of the emitters would require irradiation with an ion beam with well-defined energy that preferentially generates color centers in the lower half of the pillars,[27] whereas lateral control can be achieved by the premasking of an array of apertures.[15] Another possibility to enhance the negatively charged[18] V_{Si} yield at a desired position could lie in local doping control, as it was demonstrated, for example, with delta-doping for NV-centers in diamond.[28] Finally, focused ion beam irradiation can be applied to each fabricated nanopillar to generate color centers at a desired location, as has been recently demonstrated in diamond systems.[29]

■ ASSOCIATED CONTENT

Supporting Information

The Supporting Information is available free of charge on the ACS Publications website at DOI: 10.1021/acs.nanolett.6b05102.

Additional modeling, spectroscopic and setup information (PDF)

■ AUTHOR INFORMATION

Corresponding Authors

*E-mail: marina.radulaski@stanford.edu.

*E-mail: m.widmann@physik.uni-stuttgart.de.

ORCID

Marina Radulaski: 0000-0001-9606-3716

Author Contributions

All authors have given approval to the final version of the manuscript. M.R. and M.W. contributed equally.

Funding

This work is supported by the National Science Foundation DMR Grant 1406028, by the Army Research Office under contract W911NF1310309, by the German Federal Ministry of Education and Research (BMBF) through the ERA.Net RUS Plus Project DIABASE, and by the JSPS KAKENHI (B) 26286047.

Notes

The authors declare no competing financial interest.

■ REFERENCES

(1) Castelletto, S.; Johnson, B. C.; Ivady, V.; Stavrias, N.; Umeda, T.; Gali, A.; Ohshima, T. *Nat. Mater.* **2013**, *13*, 151−156.

(2) Widmann, M.; Lee, S. Y.; Rendler, T.; Son, N. T.; Fedder, H.; Paik, S.; Yang, L. P.; Zhao, N.; Yang, S.; Booker, I.; Denisenko, A.; Jamal, M.; Momenzadeh, S.; Al; Gerhardt, I.; Ohshima, T.; Gali, A.; Janzen, E.; Wrachtrup, J. *Nat. Mater.* **2014**, *14*, 164−168.

(3) Seo, H.; Falk, A. L.; Klimov, P. V.; Miao, K. C.; Galli, G.; Awschalom, D. D. *Nature Commun.* **2016**, *7*, 12935.

(4) Yang, L. P.; Burk, C.; Widmann, M.; Lee, S. Y.; Wrachtrup, J.; Zhao, N. *Phys. Rev. B: Condens. Matter Mater. Phys.* **2014**, *90* (24), 241203.

(5) Christle, D. J.; Falk, A. L.; Andrich, P.; Klimov, P. V.; Hassan, J. U.; Son, N. T.; Janzén, E.; Ohshima, T.; Awschalom, D. D. *Nat. Mater.* **2014**, *14* (2), 160−163.

(6) Kraus, H.; Soltamov, V. A.; Fuchs, F.; Simin, D.; Sperlich, A.; Baranov, P. G.; Astakhov, G. V.; Dyakonov, V. *Sci. Rep.* **2014**, *4*, 5303.

(7) Casady, J. B.; Johnson, R. W. *Solid-State Electron.* **1996**, *39* (10), 1409−1422.

(8) Radulaski, M.; Babinec, T. M.; Buckley, S.; Rundquist, A.; Provine, J.; Alassaad, K.; Ferro, G.; Vučković, J. *Opt. Express* **2013**, *21* (26), 32623−32629.

(9) Radulaski, M.; Babinec, T. M.; Müller, K.; Lagoudakis, K. G.; Zhang, J. L.; Buckley, S.; Kelaita, Y. A.; Alassaad, K.; Ferro, G.; Vučković, J. *ACS Photonics* **2015**, *2*, 14−19.

(10) Magyar, A. P.; Bracher, D.; Lee, J. C.; Aharonovich, I.; Hu, E. L. *Appl. Phys. Lett.* **2014**, *104* (5), 051109.

(11) Song, B. S.; Yamada, S.; Asano, T.; Noda, S. *Opt. Express* **2011**, *19* (12), 11084−11089.

(12) Falk, A. L.; Buckley, B. B.; Calusine, G.; Koehl, W. F.; Dobrovitski, V. V.; Politi, A.; Zorman, C. A.; Feng, P. X. L.; Awschalom, D. D. *Nat. Commun.* **2013**, *4*, 1819.

(13) Mizuochi, N.; Yamasaki, S.; Takizawa, H.; Morishita, N.; Ohshima, T.; Itoh, H.; Isoya, J. *Phys. Rev. B: Condens. Matter Mater. Phys.* **2002**, *66* (23), 235202.

(14) Kato, S.; Chonan, S.; Aoki, T. *Opt. Lett.* **2014**, *39* (4), 773−776.

(15) Wang, J.; Zhou, Y.; Zhang, X.; Liu, F.; Li, Y.; Li, K.; Liu, Z.; Wang, G.; Gao, W. 2016 arXiv.org 1610.03978.

(16) Fuchs, F.; Stender, B.; Trupke, M.; Simin, D.; Pflaum, J.; Dyakonov, V.; Astakhov, G. V. *Nat. Commun.* **2015**, *6*, 7578.

(17) Sörman, E.; Son, N. T.; Chen, W. M.; Kordina, O.; Hallin, C.; Janzén, E. *Phys. Rev. B: Condens. Matter Mater. Phys.* **2000**, *61*, 2613.

(18) Janzén, E.; Gali, A.; Carlsson, P.; Gällström, A.; Magnusson, B.; Son, N. T. *Phys. B* **2009**, *404* (22), 4354−4358.

(19) Niethammer, M.; Widmann, M.; Lee, S.-Y.; Stenberg, P.; Kordina, O.; Ohshima, T.; Son, N. T.; Janzén, E.; Wrachtrup. *Phys. Rev. Appl.* **2016**, *6* (3), 034001.

(20) Lee, S. Y.; Niethammer, M.; Wrachtrup. *Phys. Rev. B: Condens. Matter Mater. Phys.* **2015**, *92* (11), 115201.

DOI: 10.1021/acs.nanolett.6b05102
Nano Lett. XXXX, XXX, XXX−XXX

(21) Lohrmann, A.; Iwamoto, N.; Bodrog, Z.; Castelletto, S.; Ohshima, T.; Karle, T. J.; Gali, A.; Prawer, S.; McCallum, J. C.; Johnson, B. C. *Nat. Commun.* **2015**, *6*, 7783.
(22) Lienhard, B.; Schröder, T.; Mouradian, S.; Dolde, F.; Tran, T. T.; Aharonovich, I.; Englund, D. R. *Optica* **2016**, *3*, 768−774.
(23) Saddow, S. E. *Silicon carbide biotechnology: a biocompatible semiconductor for advanced biomedical devices and applications* Elsevier, 2012.
(24) Simin, D.; Soltamov, V. A.; Poshakinskiy, A. V.; Anisimov, A. N.; Babunts, R. A.; Tolmachev, D. O.; Mokhov, E. N.; Trupke, M.; Tarasenko, S. A.; Sperlich, A.; Baranov, P. G. *Phys. Rev. X* **2016**, *6*, 31014.
(25) Soykal, Ö. O.; Dev, P.; Economou, S. E. *Phys. Rev. B: Condens. Matter Mater. Phys.* **2016**, *93* (8), 081207.
(26) Baranov, P. G.; Bundakova, A. P.; Soltamova, A. A.; Orlinskii, S. B.; Borovykh, I. V.; Zondervan, R.; Verberk, R.; Schmidt, J. *Phys. Rev. B: Condens. Matter Mater. Phys.* **2011**, *83* (12), 125203.
(27) Babinec, T. M.; Hausmann, B. J.; Khan, M.; Zhang, Y.; Maze, J. R.; Hemmer, P. R.; Lončar, M. *Nat. Nanotechnol.* **2010**, *5* (3), 195−199.
(28) Ohno, K.; Joseph Heremans, F.; Bassett, L. C.; Myers, B. A.; Toyli, D. M.; Bleszynski Jayich, A. C.; Palmstrøm, C. J.; Awschalom, D. D. *Appl. Phys. Lett.* **2012**, *101*, 082413.
(29) Schröder, T.; Trusheim, M. E.; Walsh, M.; Li, L.; Zheng, J.; Schukraft, M.; Pacheco, J. L.; Camacho, R. M.; Bielejec, E. S.; Sipahigil, A.; Evans, R. E. 2016, arXiv.org 1610.09492.

DOI: 10.1021/acs.nanolett.6b05102
Nano Lett. XXXX, XXX, XXX−XXX